nature nanotechnology

REVIEW ARTICLE

PUBLISHED ONLINE: 13 SEPTEMBER 2009 | DOI: 10.1038/NNANO.2009.242

Towards a definition of inorganic nanoparticles from an environmental, health and safety perspective

Mélanie Auffan[1,3], Jérôme Rose[1,2,3], Jean-Yves Bottero[1,2,3], Gregory V. Lowry[1,3,4], Jean-Pierre Jolivet[1,3,5] and Mark R. Wiesner[1,3*]

The regulation of engineered nanoparticles requires a widely agreed definition of such particles. Nanoparticles are routinely defined as particles with sizes between about 1 and 100 nm that show properties that are not found in bulk samples of the same material. Here we argue that evidence for novel size-dependent properties alone, rather than particle size, should be the primary criterion in any definition of nanoparticles when making decisions about their regulation for environmental, health and safety reasons. We review the size-dependent properties of a variety of inorganic nanoparticles and find that particles larger than about 30 nm do not in general show properties that would require regulatory scrutiny beyond that required for their bulk counterparts.

An engineered nanoparticle may be defined as any intentionally produced particle that has a characteristic dimension from 1 to 100 nm and has properties that are not shared by non-nanoscale particles with the same chemical composition. Although the first part of this fairly broadly accepted definition[1–4] specifies a size range, which is often the focal point in defining nanoparticles, we will argue that the second part is more relevant when considering the impact of nanoparticles on the environment and human health. The central question is this: do nanoparticles have properties affecting either exposure or hazard that are fundamentally different from those shown by larger particles of identical composition? This remains an open question.

Although nanoparticles may be more easily taken up by organisms through ingestion, respiration or both, which potentially increases their residence time and exposure in environmental systems (see, for example, refs 5 and 6), these effects typically result from their small size (an extrinsic property) rather than a unique nanoscale property (an intrinsic property). New fundamental physics or theories beyond those encompassed by colloid chemistry are not necessarily needed to describe the interactions of particles in the 1–100-nm size range with other materials in the biosphere. However, the 'non-bulk' properties of nanoparticles, their atypical surface structure and their reactivity (the second part of the definition) may enhance processes such as dissolution, redox reactions or the generation of reactive oxygen species (ROS; see, for example, refs 7–9). Such properties may be accompanied by biological effects that would not be produced by larger particles of the same chemical composition. In these cases, new approaches are needed to systematically define nanoparticles and their properties (for example, structural characterization) as a basis for ensuring the reproducibility of results, identifying underlying mechanisms of toxicity and predicting environmental behavior[2,10,11].

We focus here on inorganic metal and metal oxide nanoparticles for which there is substantial interest in commercial development[12–19] as well as concerns surrounding their (eco)toxicological impacts[6,20–29]. We conclude that there is a critical size, considerably smaller than 100 nm, for which these new properties typically appear (Fig. 1a). This critical size is strongly related to the exponential increase in the number of atoms localized at the surface as the size decreases (Fig. 1b) and delineates a smaller set of nanoparticles (typically with diameters less than 20–30 nm). These smaller nanoparticles have a size-dependent crystallinity that gives them properties drastically different from the bulk material and they fit the two-part definition discussed above[30–35]. These observations suggest that nanotoxicological studies might be better focused on a smaller set of nanoparticles that show unique nanoscale properties.

Size, crystallinity and thermodynamics

Nanoparticles below 20–30 nm in size are characterized by an excess of energy at the surface and are thermodynamically unstable[36]. Crystallographic changes (for example lattice contraction or deformation, the appearance of defects, rearrangements of the surface atoms or changes in morphology)[37–41] may occur to stabilize them. These unique nanoscale features affect the interfacial reactivity and the intrinsic properties of nanoparticles. The size dependence of the optical and electronic properties of quantum dots provides a clear example. The bandgap energy (corresponding to the fluorescence wavelength) abruptly increases as diameter decreases below 6–8 nm (Fig. 2a). These properties are attributed to lattice contractions[42] that favour the confinement of electrons and the existence of discrete electronic states that are virtually absent for larger particles[43–45]. Another example is the size dependence of thermal properties of nanoparticles[46]. The melting point of indium and tin nanoparticles can be respectively reduced by 120 °C (ref. 47) and 80 °C (ref. 34) by decreasing their diameters from 100 nm to 10 nm, with an exponential drop for sizes below 15 nm (Fig. 2b). Moreover, the normalized heat of fusion, ΔH_m, behaves in a similar way (Fig. 2b), whereas it is assumed to be constant in classical thermodynamics. This enhancement is attributed to an increasing fraction of lattice defects and irregularities in the crystalline structure of the nanoparticles[48]. Electric and magnetic properties are also known to be related to the size and the crystallinity[49–51]. For instance, size-dependent changes of the transition temperature — be it the Curie temperature for ferromagnetic particles ($MnFe_2O_4$ and $MgFe_2O_4$), the Néel temperature

---

[1]Center for the Environmental Implications of NanoTechnology CEINT, Duke University, 121 Hudson Hall, Durham, North Carolina 27707, USA, [2]CEREGE, UMR 6635 CNRS/Aix-Marseille Université, Europôle de l'Arbois, 13545 Aix-en-Provence, France, [3]International Consortium for the Environmental Implications of Nanotechnology iCEINT, Europôle de l'Arbois, 13545 Aix-en-Provence, France, [4]Carnegie Mellon University, Civil and Environmental Engineering Department, 119 Porter Hall, Pittsburgh, Pennsylvania 15213, USA, [5]Laboratoire de Chimie de la Matière Condensée de Paris, UMR 7574 CNRS/UPMC, Jussieu, 75252 Paris, France. *e-mail: wiesner@duke.edu

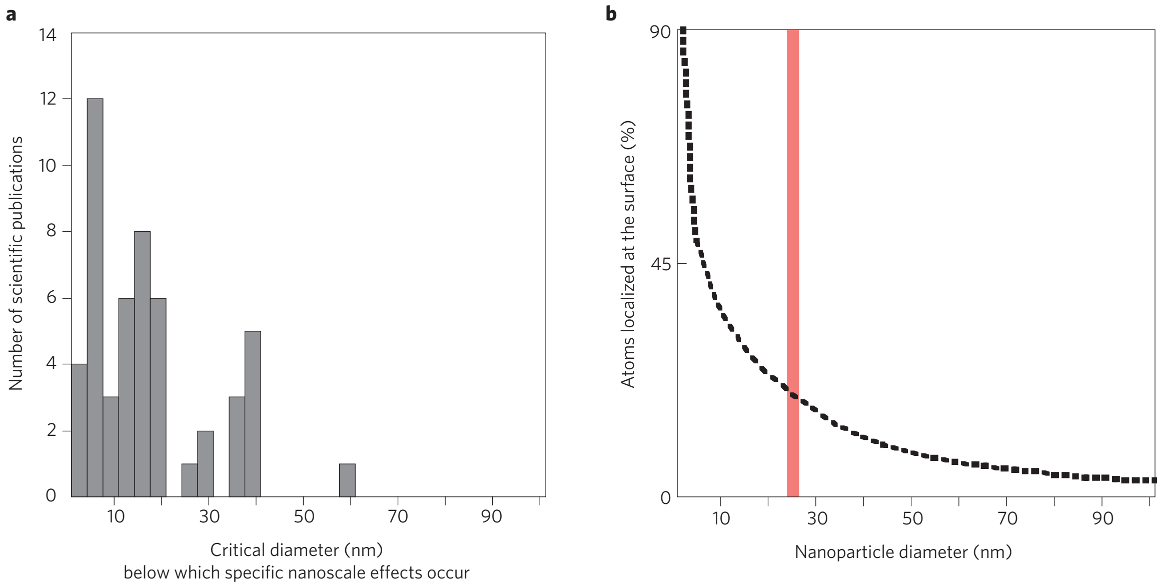

Figure 1 | Below what size do nanoparticles show properties not seen in larger particles with the same chemical composition? a, The number of published papers (vertical axis) reporting non-bulk properties in nanoparticles below a certain size plotted against the size of the nanoparticles (horizontal axis). **b**, The percentage of atoms localized at the surface of a nanoparticle as a function of the nanoparticle diameter. We argue that non-bulk properties only emerge for diameters of less than 20–30 nm (red line).

for antiferromagnetic particles ($BiFeO_3$)[35,52–54] or the paraelectric-to-ferroelectric transition temperature (for example in $PbTiO_3$)[55,56] — have been observed only for sizes less than 20–30 nm. In the case of $PbTiO_3$ particles, the decrease in the transition temperature by about 20 °C (for sizes between 80 and 30 nm) is accompanied by a pronounced decrease in the ratio c/a (where c and a are the lattice parameters), indicating a tetragonal distortion of the crystalline unit cell.

Most of the size effects are predictable in part from thermodynamics, as this is a direct consequence of the Laplace equation, but they are strongly pronounced once the size is significantly below 100 nm (ref. 57). A distinctive feature of very small nanoparticles (<30 nm) is that the surface tension, γ, depends on the size, r, and the derivative $d\gamma/dr$ must be taken into account in thermodynamic models[57]. For instance, this size dependence of γ is of great importance in two physicochemical processes (dissolution and phase transformation) that need to be accounted for or controlled in nanotoxicological studies[58].

The driving force for dissolution depends on the crystal solubility within a given environment (for example, in water with low ionic strength or in cellular nutritive solution), the concentration gradient between the particle and the solution, the specific surface area (SSA) and the aggregation state[10,58]. It is intuitive that for a given mass, the dissolution kinetics is proportional to the SSA, with faster dissolution predicted for nanoparticles than for larger particles. The main question concerns the potential size dependence of the crystal solubility, K_b. From a thermodynamic point of view, K_b is assumed to be constant and is routinely approximated using the solubility product, K_{sp}, according to $\ln K_b = \ln K_{sp} + c(\gamma/l)$, where l is the characteristic dimension of the crystal and $c = 2\tau W/\rho RT$ (τ is the geometrical factor of the nucleus, W is the molecular weight, ρ is the density, R is the gas constant and T is the absolute temperature). However, this approach fails to describe the solubility of crystals smaller than 25 nm (ref. 59). Whereas replacing K_b with K_{sp} is a reasonable approximation when the particles are large, the size dependence of the morphology, γ and the activation energies of the dissolution process[60] cannot be ignored in the case of very small nanoparticles[59–61]. This will modify the chemical stability of nanoparticles smaller than 20–30 nm in solution and thus affect their toxicity. As with the dissolution process, solid-phase transitions of nanoparticles are also related to the size dependence of γ. If γ is increased, the pressure inside particles increases and the phase-transition temperature decreases[57]. For instance, as a ZrO_2 particle decreases in size to 10 nm, the monoclinic form is transformed to the tetragonal one at room temperature, whereas a monoclinic–tetragonal modification occurs on heating to 1,100 °C for bulk ZrO_2. It was also shown that γ-Al_2O_3 (the phase observed for nanoparticles) is enthalpically more stable than α-Al_2O_3, the thermodynamically stable phase of the larger particles[62]. It has also been proposed that the surface enthalpies of the three TiO_2 polymorphs (2.2 ± 0.2, 1.0 ± 0.2 and 0.4 ± 0.1 J m^{-2}, respectively, for rutile, brookite and anatase) are sufficiently different that crossover in thermodynamic stability can occur under conditions that preclude coarsening, with anatase and/or brookite stable at small size[63,64].

Crystallinity and size-dependent interfacial properties

Recent studies provide strong evidence that nanoparticles can not only passively interact with cells[20,26,28,65], but also actively engage and mediate molecular processes that are essential for regulating cell functions[66]. The interfacial properties of inorganic nanoparticles in solution, including the rates of reactions mediated on the surface, adsorption capacity and change of redox state[67–69], are likely to affect the fate of nanoparticles in the environment and possibly toxicity in organisms. Hence, a size-dependent change in crystallinity related to the decrease in the excess of surface free energy for nanoparticles smaller than 20 nm can enhance the interfacial reactivity and modify their reactivity in the environment. Relating size-dependent modifications of the particles' surface properties to associated changes in reactivity at the nanoscale remains an important challenge. In the following sections, the properties of different nanoparticles are presented to illustrate the influence of the nanoscale on the interfacial reactivity.

Crystallinity and reactivity of Fe^0. Crystalline particles have long-range order resulting from repeating unit cells. There are reported cases in which amorphous particles are more reactive than their crystalline counterparts. For example, amorphous

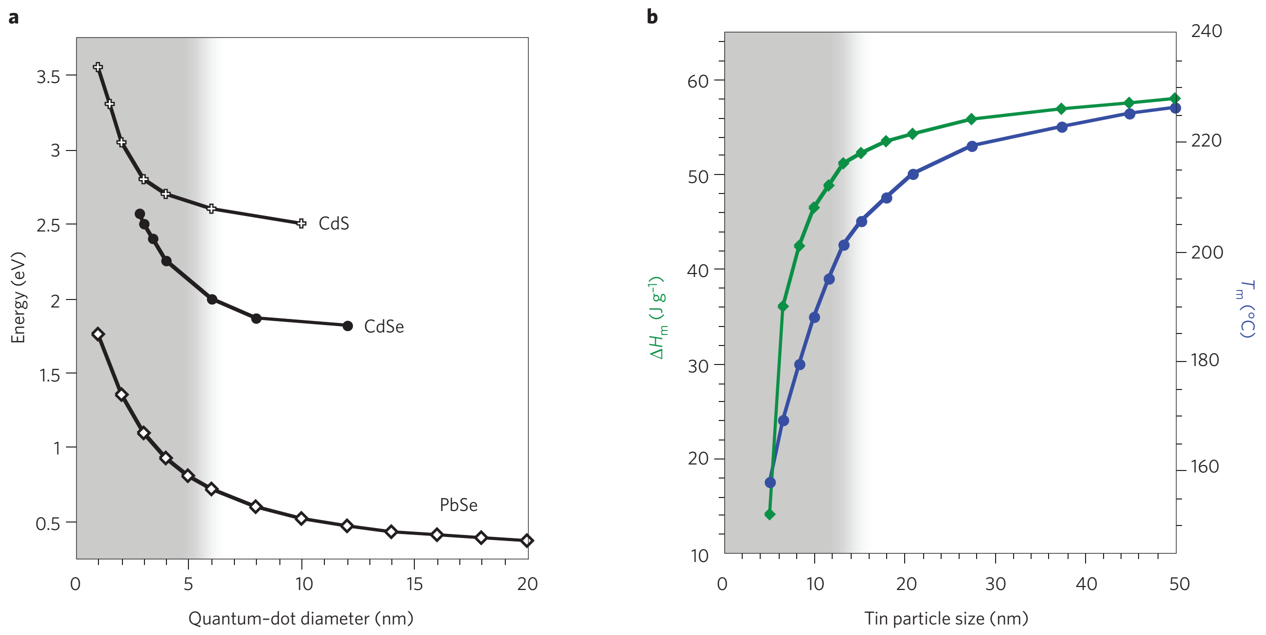

Figure 2 | Size dependence of various physical properties of nanoparticles. a, The bandgap energy of PbSe, CdSe and CdS quantum dots as a function of diameter (adapted from refs 30–33). The bandgap energy of a system determines its electronic and optical properties. **b**, The melting temperature (T_m; green line) and heat of fusion (ΔH_m; blue line) of tin particles as a function of diameter (adapted from ref. 34). The grey areas correspond to the size range in which the properties change significantly. The bandgap changes greatly for diameters below about 6 nm, whereas the thermal properties start to change below about 15 nm.

ribbons of metal–boron alloy were more reactive than crystalline ribbons with the same composition in the catalytic hydrogenation of carbon monoxide[70]. More recently, it was demonstrated that 20–40-nm amorphous Fe^0 particles possessed the ability to activate and use dissolved H_2 for the aqueous-phase hydrodechlorination of trichloroethylene[71]. Particles annealed to a crystalline form lacked this ability. The Fe^0 nanoparticles studied, however, were X-ray amorphous (Cu Kα source) and had a broad X-ray diffraction peak ($2\theta = 45°$); the presence of α-Fe^0, with larger crystals would have produced a narrow peak. Closer examination of those particles (using dark-field tunnelling electron microscope imaging) indicated that there were α-Fe^0 crystallites on the order of 1–2 nm in size within the larger, apparently amorphous particles[72]. Thus, although they are X-ray amorphous, the particles indeed have short-range order on the scale of a few unit cells (~64 unit cells per 1-nm crystallite). The high surface energy and high defect rate in these 1–2-nm α-Fe^0 crystallites most probably afforded them an ability to activate and use H_2, whereas 20–70-nm crystallites of Fe^0 cannot activate H_2 (ref. 73).

Morphology and interfacial reactivity of boehmite. In the environment, crystallized particles show different faces that are more or less chemically active. A size-dependent change in morphology can strongly influence the ratio between the crystallographic planes and modify the interfacial reactivity. This was observed for boehmite (γ-AlOOH) particles ranging in size between 10 and 100 nm (ref. 74). Particles of γ-AlOOH 100 nm in size are fibres or rods formed by aggregation of very small platelets (3 nm thick and 6 nm wide) with (100) lateral faces and (010) basal planes. Conversely, γ-AlOOH nanoparticles between 10 and 25 nm in size are diamond-shaped with (101) lateral faces as suggested by the angle of ~104° between the (101) and (10–1) distortions. Hence, when the size decreases, a change in the area ratio between the (100), (010) and (101) faces occurs as a result of modifications in the electrostatic surface charge density and in the surface energy[36]. This is an important feature of γ-AlOOH particles because they are the precursor of γ-Al_2O_3, which is widely used as a catalyst support for metal[75,76]. As the thermal transformation γ-AlOOH → γ-Al_2O_3 is topotactic (that is, it maintains the morphology of the particles), the control of the shape of the 10-nm γ-AlOOH particles enables the development of corresponding faces on γ-Al_2O_3 and therefore the adjustment of their interfacial reactivity towards a given reaction[77].

Phase transformation and photocatalysis by titanium dioxide. As previously mentioned, solid-phase transformations may be size dependent[38], reflecting, for example, the size dependence of the photocatalytic activity of TiO_2. The anatase phase, which is greater for very small TiO_2 particles, is more effective in the production of hydroxyl radicals and the subsequent decomposition of organic compounds than the rutile phase. It is interesting to note that this size-dependent photocatalytic activity does not increase monotonically with decreasing size but rather passes through a maximum significantly below 100 nm. This size is ~7 nm for trichloroethylene[78], ~11 nm for chloroform[79] and ~25 nm for phenol[80]. These optimum sizes are thought to result from competing effects of the particle size on light absorption and scattering efficiency, charge-carrier dynamics and SSA.

Electronic structure and catalytic activity of gold. The size-dependent electronic and structural properties of metal particles on oxide supports are important features of heterogeneous catalysis[81]. One of the most fascinating examples is gold particles[82]. Although gold is known to be inert at the macroscopic scale, when their size is reduced to a few nanometres gold nanoparticles are extremely effective oxidation catalysts[83–85]. A threshold in size near 2 nm has been observed, above which gold particles are completely inactive as catalysts for the epoxidation of styrene by dioxygen[86]. This reaction needed no initiator and the support medium was inert, so the effect seems to involve size-dependent changes in the properties of gold. Although the origin of this behaviour is not yet fully understood; the catalytic activity seems

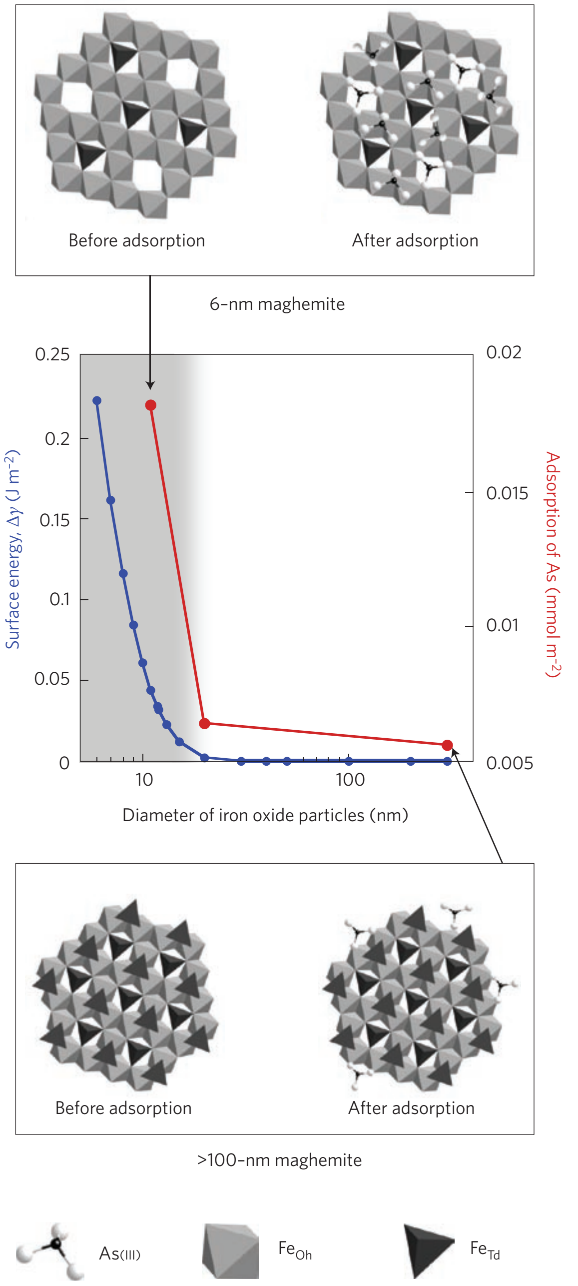

Figure 3 | Size dependence of the mechanisms of arsenic adsorption at the surface of iron oxide particles. The graph shows how the adsorption capacity of As(III) at the surface of Fe_3O_4 nanoparticles (red line; adapted from ref. 90) and the surface free energy after saturation of all the adsorption sites at the surface (blue line; adapted from ref. 36) vary with diameter (on a logarithmic scale). Both quantities start to change significantly for diameters below about 20 nm (grey area). The evolution of the crystalline structure of the *hkl* plane (111) of maghemite particles and the mechanisms for the adsorption of arsenic at the surface are shown for 6-nm particles (top) and >100-nm particles (bottom: adapted from ref. 68). Fe_{Oh}, octahedral iron; Fe_{Td}, tetrahedral iron.

to arise from the size-dependent alteration of electronic structure. A shift (of 1.1 eV) in the $4f_{7/2}$-electron apparent binding energy of gold nanoparticles was noted relative to larger gold particles. Moreover, independent of the support and only for nanoparticles smaller than 3 nm, decreasing particle size was associated with an increase in the 3*d*-electron density of the gold atoms and the onset of reactivity with oxygen in air[87]. This suggests that the size-dependent alteration of electronic structure gives rise to unusual catalytic properties.

Atomic rearrangement and adsorption by iron oxide. One approach to studying the distribution of the atoms at the surfaces of particles is to use specific chemical species to probe surface sites for size dependence of reactivity[68,88,89]. Arsenic has been used to probe the size-dependent surface properties of iron oxide particles. The quantity of arsenic adsorbed per gram of iron oxide has been observed to increase from 0.02 to 1.8 mmol g^{-1} as particles size decreases from 300 to 11 nm (ref. 90). Much of this 100-fold increase of adsorption capacity can be attributed to a simple surface-area effect[74]. However, a comparison of the adsorbed quantity per mass of particles reveals nothing about the chemical reactivity or the relative affinity. When normalized by SSA, 300-nm and 20-nm iron oxide particles are observed to adsorb similar amounts of arsenic (~6 μmol m^{-2} or 3.6 atoms nm^{-2}), suggesting that similar adsorption mechanisms are involved over this size range. Surprisingly, for particles smaller than 20 nm, the adsorption capacity increases, with 11-nm magnetite particles adsorbing three times more arsenic per square nanometre (~18 μmol m^{-2} or 11 atoms nm^{-2}) than do 20-nm iron oxide particles[90] (Fig. 3).

These large values cannot be solely attributed to the increase in the number of surface reactive sites, which is limited by the size of the atoms (the maximum number of molecules adsorbed onto the surface is estimated at ~4 atoms nm^{-2} (refs 91, 92)). Only a change in the surface structure leading to the appearance of new surface adsorption sites and a significant decrease of the surface energy[36,93] can explain the enhanced adsorption capacity. This was observed for the first time at the surfaces of maghemite (γ-Fe_2O_3) particles[40,68]. As the size decreased, the occupancy of the tetrahedral ($[Fe_{Td}]$) site decreased, creating unique and highly reactive adsorption sites in the crystal lattice position available to adsorb a large number of ions, for instance 8–10 As(III) atoms per square nanometre[68]. Two mechanisms of As(III) adsorption appear to dominate as a function of the surface coverage (Fig. 3). At low surface coverage, arsenic fills the more reactive $[Fe_{Td}]$ surface sites in an octahedral ring (As(III) is surrounded by six $[Fe_{Oh}]$ atoms). When all of these sites are filled, As(III) fills the less reactive $[Fe_{Td}]$ sites and is adsorbed on a $[Fe_{Oh}]$ trimer through monodentate trinuclear complexes in a lattice position. For larger γ-Fe_2O_3 particles, all $[Fe_{Td}]$ sites are occupied, which decreases the number of possible adsorption sites. Moreover, it is interesting to note that the γ-Fe_2O_3 nanoparticles used in ref. 68 were obtained from acidic treatment of magnetite (Fe_3O_4) nanoparticles. This transformation is facilitated at the nanoscale by an easy structural change allowing the complete desorption of Fe^{2+} ions from the nanoparticles[94].

Interfacial properties and biological effects

In the context of risk assessment, novel size-dependent properties that influence nanoparticle reactivity are likely to affect both nanoparticle exposure and hazard. Sources of reactivity may include affinity for electron uptake (perhaps from bacterial electron carriers) and subsequent transfer to species in solution[58], aggregation[10] and interfacial phenomena such as adsorption of pollutants[68] or naturally occurring macromolecules[66]. It is likely that such factors can play an important part in the toxicity of inorganic nanoparticles through mechanisms such as transformation of chemical species, the production of ROS and the release of toxic species into solution[20,26,28,65].

Generation of ROS and oxidative stress. The presence of active sites on nanoparticles that are able to generate ROS and arise from size-dependent differences in atomic and electronic structure suggests one possible origin of a size dependence in toxicity. Several authors have shown that the ROS generation is involved in the toxicity of nanoparticles (for example CeO_2, TiO_2, nC_{60}, Fe_3O_4 and Fe^0). Direct relationships between the SSA, the generation of ROS and the inflammatory effects induced by nanoparticles have been shown[20]. However, it is not clear whether size-dependent structural changes contribute to an increase of toxicity in a general sense (see, for example, refs 95, 96). For instance, for a given mass, 20-nm anatase TiO_2 nanoparticles are more toxic towards rats than are 250-nm anatase particles. For a given SSA, however, the toxicity responses are similar for all the sizes studied[6]. A number of the present authors have demonstrated that, per unit mass, 7-nm CeO_2 nanoparticles induced stronger oxidative stress and greater damage to DNA and chromosomes *in vitro* than did 300-nm CeO_2 particles[7], but once normalized by the SSA no significant difference exists. Hence, these examples do not suggest a size-dependent increase in biological effects.

However, other studies have reported anatase (present in greater proportions for TiO_2 crystallites <15 nm in size) to be more biologically active than rutile TiO_2 in terms of cytotoxicity or oxidative DNA damage[97,98]. It has been shown[99] that the bactericidal effects increase as the size of nanoparticles decreases from 30 to 15 nm and the mass fraction of anatase increases. Furthermore, it was recently demonstrated[100] that 100% anatase nanoparticles, regardless of size, induce cell necrosis and membrane leakage, but they do not generate ROS. In contrast, the rutile nanoparticles initiate apoptosis through formation of ROS. Therefore, it seems that links between size and crystal structure may have a role in mediating nanoparticle toxicity.

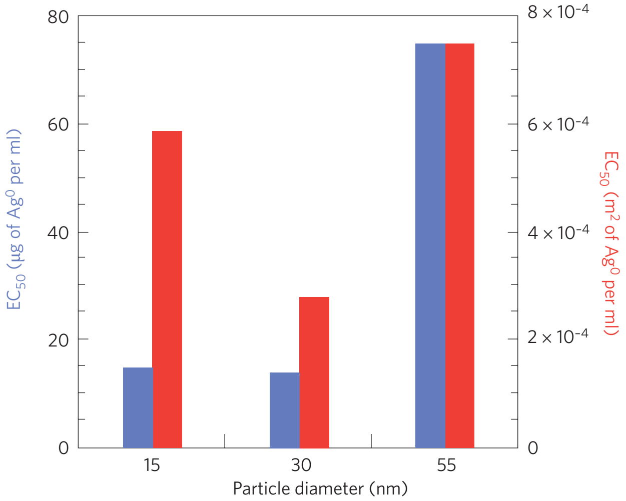

Figure 4 | Toxicity of silver nanoparticles. Cytotoxicity data for three different sizes of silver nanoparticle normalized by mass (blue; left-hand axis) and surface area (red; right-hand axis). The EC_{50} values represent the effective concentration of silver nanoparticles required to decrease by 50% the membrane integrity (assessed by measuring lactate dehydrogenase leakage; adapted from ref. 8). The SSAs of the 55-nm, 30-nm and 15-nm nanoparticles were estimated to be 10, 20 and 40 $m^2\ g^{-1}$, respectively.

Dissolution and release of toxic ions. The importance of the chemical stability of metal or metal oxide nanoparticles on their toxicity *in vitro* has been demonstrated recently[101]. Chemically unstable nanoparticles can be oxidized, reduced and dissolved in biological media, leading to the release of toxic ions. Nanoparticles that show a higher solubility in cellular growth media (such as ZnO nanoparticles) show a stronger toxicity to mammalian cells than do nanoparticles with a low solubility (such as TiO_2)[102]. The biological impacts of ZnO nanoparticles *in vitro* result from the release of Zn^{2+} and $Zn(OH)^+$ ions, which are the dominant species in fresh water of moderate alkalinity and neutral pH[103]. This is confirmed by toxicity studies performed on the freshwater alga *Pseudokirchneriella subcapitata*, which reveal comparable toxicity of 30-nm ZnO and dissolved $ZnCl_2$ salts[104]. The toxicity attributed to CdSe quantum dots is also mediated by their intracellular oxidation and the release of Cd^{2+} and Se^{2-} ions. This acute cytotoxicity is reduced when metal dissolution is limited by coating the surface[105].

Particle dissolution processes known to affect the toxicity of non-nanoscale particles are not clearly applicable to nanoparticles. Solubility is highly dependent on solvent properties (for example pH, ionic strength and the presence of adsorbing species) and on the particles properties (for example SSA, surface morphology, surface energy and reactivity, and aggregation states)[58]. However, as previously discussed, the dissolution can be enhanced at the nanoscale as the result of size-dependent structural changes. It has been found that the bactericidal effect of silver nanoparticles between 1 and 100 nm in diameter was highest in the 1–10-nm range, where there are more highly reactive {111} surfaces[106]. These particles penetrate bacteria, strongly interact with sulphur- and phosphorus-containing compounds and release toxic silver ions.

Dose-response assessment per gram and per square nanometre. The previous examples highlight the necessity of comparing the dose-response effects of different sizes of nanoparticle in two ways: per unit of mass and per unit of surface area. A size dependence of toxicity induced by silver nanoparticles has been observed[8] when the cytotoxicity data are mass weighted (Fig. 4). Once normalized by the SSA, the results are more surprising because as a function of the cytotoxic assays used, the 30-nm and 15-nm silver nanoparticles remain more toxic than the 55-nm silver nanoparticles (Fig. 4). This is in contradiction with other studies showing no size effect when the data are surface weighted[6,107] or even mass weighted[108], and it also highlights how little we know about the relationship between the size and the biological effect. All things considered, these examples illustrate that performing experiments with particles in the range 1–100 nm is not sufficient for the purposes of identifying biochemical mechanisms that may differ from those observed with larger particles, because the relevant properties are likely to vary significantly across this range of sizes. Moreover, in physiological media nanoparticles are likely to undergo significant modifications (for example aggregation, surface passivation)[10] that may obscure the relationship between their unique, size-dependent properties and their biological effects.

In some cases, the intrinsic properties of the nanoparticles may be more closely related to processes that control nanoparticle modifications or transformations to other chemical species present, rather than direct cellular effects by the nanoparticles themselves. These factors will complicate efforts seeking to relate nanoparticle properties to biological effects using a quantitative structure–activity relationship (QSAR)-type approach as well as efforts to 'tune' the toxicity of nanoparticles by chemical modification of their surfaces. However, an understanding of nanoparticle toxicity must consider underlying changes in intrinsic properties that occur at the nanoscale as a basis for differentiating these materials from their bulk counterparts. Focusing on size-related properties, rather than on size alone, has important implications for the design of research programmes to evaluate the safety of engineered inorganic nanoparticles. Indeed, ignoring the differences between that which is merely small and that which is truly 'nano' may obscure the interpretation of experimental results.

Conclusion

A definition of nanoparticles based on their non-bulk size-dependent properties is needed to better focus future research efforts in

NATURE NANOTECHNOLOGY DOI: 10.1038/NNANO.2009.242

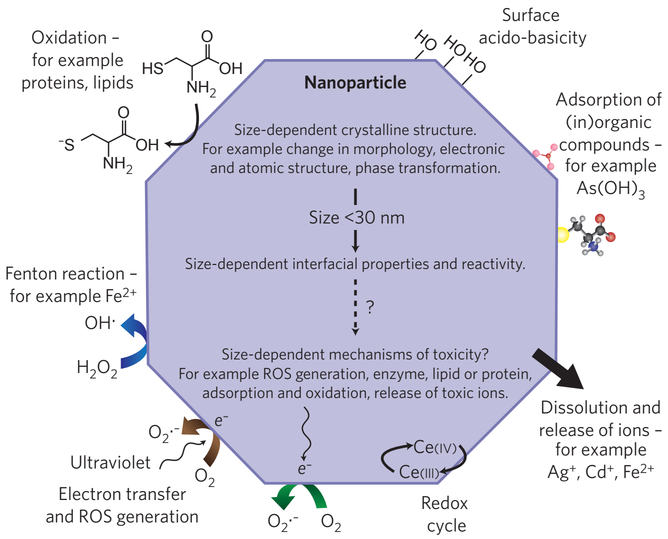

Figure 5 | A number of physicochemical mechanisms can occur at the surface of an inorganic nanoparticle. The potential relationship between the size dependence of the crystalline structure of nanoparticles (typically <30 nm), their interfacial properties (for example dissolution, oxidation, adsorption/desorption, electron transfer, redox cycles, Fenton reactions and surface acido-basicity) and potential mechanisms of toxicity (for example, the generation of ROS, the release of toxic ions, the oxidation of proteins and the adsorption of pollutants). OH·, hydroxyl radical; $O_2^{\cdot -}$, anion superoxide.

nanotoxicology, and to compare the results of studies performed on particles of identical composition. The weight of evidence from the literature suggests that engineered nanoparticles are likely to be of concern owing to unique properties when they have diameters of 30 nm or less. In this size range, many particles undergo dramatic changes in crystalline structure that enhance their interfacial reactivity (Fig. 5).

Although there are several examples of particle toxicity scaling with surface area[6], it is not clear whether this is associated with unique properties of exposure or hazard that merit special consideration in terms of mechanisms of activity and potential toxicity compared with larger particles. For instance, does the appearance of catalytic properties at the nanoscale interfere with the electronic transfers within the respiratory chain? Is a size-dependent generation of ROS able to enhance the breakage of DNA strands? Is the enhanced adsorption capacity of nanoparticles smaller than 30 nm able to increase the adsorption or inactivation of proteins? Is there a size-dependence in the inflammatory response and genotoxicity? To answer these questions, nanotoxicological studies should contrast particles that have novel size-dependent properties, particularly concerning their surface reactivity, and those particles that do not show these properties.

References

1. Académie des Sciences, Académie des Technologies. *Nanosciences - Nanotechnologies*. Science and Technology Report No. 18 (French Academy of Sciences, 2004); summary of recommendations (in English) available at <http://www.tinyurl.com/nqwdda>.
2. The Royal Society and The Royal Academy of Engineering. *Nanoscience and Nanotechnology: Opportunities and Uncertainties* (The Royal Society, 2004); available at <http://www.nanotec.org.uk>.
3. Hansen, S. F., Larsen, B. H., Olsen, S. I. & Baun, A. Categorization framework to aid hazard identification of nanomaterials. *Nanotoxicology* **1,** 243–250 (2007).
4. Nanoscale Science Engineering and Technology Subcommittee. *The National Nanotechnology Initiative: Strategic Plan* (US National Science and Technology Council, 2004); available at <http://www.nano.gov/NNI_Strategic_Plan_2004.pdf>.
5. Donaldson, K., Stone, V., Tran, C. L., Kreyling, W. & Born, P. J. A. Nanotoxicology. *Occup. Environ. Med.* **61,** 727–728 (2004).
6. Oberdörster, G., Oberdörster, E. & Oberdörster, J. Nanotoxicology: an emerging discipline evolving from studies of ultrafine particles. *Environ. Health Perspect.* **113,** 823–839 (2005).
7. Auffan, M. *et al.* CeO$_2$ nanoparticles induce DNA damage towards human dermal fibroblasts *in vitro*. *Nanotoxicology* **3,** 161–171 (2009).
8. Carlson, C. *et al.* Unique cellular interaction of silver nanoparticles: size-dependent generation of reactive oxygen species. *J. Phys. Chem. B* **112,** 13608–13619 (2008).
9. Xia, T. *et al.* Comparison of the abilities of ambient and manufactured nanoparticles to induce cellular toxicity according to an oxidative stress paradigm. *Nano Lett.* **6,** 1794–1807 (2006).
10. Murdock, R. C., Braydich-Stolle, L., Schrand, A. M., Schlager, J. J. & Hussain, S. M. Characterization of nanomaterial dispersion in solution prior to *in vitro* exposure using dynamic light scattering technique. *Toxicol. Sci.* **101,** 239–253 (2008).
11. Billinge, S. J. L. & Levin, I. The problem with determining atomic structure at the nanoscale. *Science* **316,** 561–565 (2007).
12. Bottero, J. Y., Rose, J. & Wiesner, M. R. Nanotechnologies: tools for sustainability in a new wave of water treatment processes. *Integr. Environ. Assess. Manag.* **2,** 391–395 (2006).
13. Emerich, D. F. & Thanos, C. G. The pinpoint promise of nanoparticle-based drug delivery and molecular diagnosis. *Biomol. Eng.* **23,** 171–184 (2006).
14. Gupta, A. K. & Gupta, M. Synthesis and surface engineering of iron oxide nanoparticles for biomedical applications. *Biomaterials* **26,** 3995–4021 (2005).
15. Pereira de Abreu, D. A., Paseiro Losada, P., Angulo, I. & Cruz, J. M. Development of new polyolefin films with nanoclays for application in food packaging. *Eur. Polym. J.* **43,** 2229–2243 (2007).
16. Zhang, W. Nanoscale iron particles for environmental remediation: an overview. *J. Nanopart. Res.* **5,** 323–332 (2003).
17. Sahoo, S. K. & Labhasetwar, V. Nanotech approaches to drug delivery and imaging. *Drug Discov. Today* **8,** 1112–1120 (2003).
18. Kim, C. K. *et al.* Entrapment of hydrophobic drugs in nanoparticle monolayers with efficient release into cancer cells. *J. Am. Chem. Soc.* **131,** 1360–1361 (2009).
19. Xia, Y. Nanomaterials at work in biomedical research. *Nature Mater.* **7,** 758–760 (2008).
20. Nel, A., Xia, T., Madler, L. & Li, N. Toxic potential of materials at the nanolevel. *Science* **311,** 622–627 (2006).
21. Wiesner, M. R., Lowry, G. V. & Alvarez, P. J. J. Assessing the risks of manufactured nanomaterials. *Environ. Sci. Technol.* **40,** 4336–4345 (2006).
22. Lanone, S. & Boczkowski, J. Biomedical applications and potential health risks of nanomaterials: molecular mechanisms. *Curr. Mol. Med.* **6,** 651–663 (2006).
23. Moore, M. N. Do nanoparticles present ecotoxicological risks for the health of the aquatic environment? *Environ. Int.* **32,** 967–976 (2006).
24. Fortner, J. D. *et al.* C$_{60}$ in water: nanocrystal formation and microbial response. *Environ. Sci. Technol.* **39,** 4307–4316 (2005).
25. Oberdörster, E. Manufactured nanomaterials (fullerene, C$_{60}$) induce oxidative stress in the brain of juvenile largemouth bass. *Environ. Health Perspect.* **112,** 1058–1062 (2004).
26. Auffan, M. *et al.* Relation between the redox state of iron-based nanoparticles and their cytotoxicity towards Escherichia Coli. *Environ. Sci. Technol.* **42,** 6730–6735 (2008).
27. Auffan, M. *et al.* *In vitro* interactions between DMSA-coated maghemite nanoparticles and human fibroblasts: a physicochemical and cyto-genotoxical study. *Environ. Sci. Technol.* **40,** 4367–4373 (2006).
28. Thill, A. *et al.* Cytotoxicity of CeO$_2$ nanoparticles for Escherichia coli. Physico-chemical insight of the cytotoxicity mechanism. *Environ. Sci. Technol.* **40,** 6151–6156 (2006).
29. Scheufele, D. A., Corley, E. A., Shih, T.-J., Dalrymple, K. E. & Ho, S. S. Religious beliefs and public attitudes toward nanotechnology in Europe and the United States. *Nature Nanotech.* **4,** 91–94 (2009).
30. Lin, K.-F., Cheng, H.-M., Hsu, H.-C., Lin, L.-J. & Hsieh, W.-F. Band gap variation of size-controlled ZnO quantum dots synthesized by sol–gel method. *Chem. Phys. Lett.* **409,** 208–211 (2005).
31. Moreels, I. *et al.* Composition and size-dependent extinction coefficient of colloidal PbSe quantum dots. *Chem. Mater.* **19,** 6101–6106 (2007).
32. Norris, D. J. & Bawendi, M. G. Measurement and assignment of the size-dependent optical spectrum in CdSe quantum dots. *Phys. Rev. B* **53,** 16338–16346 (1996).
33. Wang, Y. & Herron, N. Quantum size effects on the exciton energy of CdS clusters. *Phys. Rev. B* **42,** 7253–7255 (1990).
34. Lai, S. L., Guo, J. Y., Petrova, V., Ramanath, G. & Allen, L. H. Size-dependent melting properties of small tin particles: nanocalorimetric measurements. *Phys. Rev. Lett.* **77,** 99–102 (1996).

35. Tang, Z. X., Sorensen, C. M., Klabunde, K. J. & Hadjipanayis, G. C. Size-dependent Curie temperature in nanoscale $MnFe_2O_4$ particles. *Phys. Rev. Lett.* **67,** 3602–3605 (1991).
36. Jolivet, J. P. *et al.* Size tailoring of oxide nanoparticles by precipitation in aqueous medium. A semi-quantitative modelling. *J. Mater. Chem.* **14,** 3281–3288 (2004).
37. Lamber, R., Wetjen, S. & Jaeger, N. I. Size dependence of the lattice parameter of small palladium particles. *Phys. Rev. B* **51,** 10968–10971 (1995).
38. Ayyub, P., Palkar, V. R., Chattopadhyay, S. & Multani, M. Effect of crystal size reduction on lattice symmetry and cooperative properties. *Phys. Rev. B* **51,** 6135–6138 (1995).
39. Banfield, J. F. & Navrotsky, A. (eds) *Nanoparticles and the Environment* (Mineralogical Society of America, 2001).
40. Brice-Profeta, S. *et al.* Magnetic order in γFe_2O_3 nanoparticles: a XMCD study. *J. Magn. Magn. Mater.* **288,** 354–365 (2005).
41. Baudrin, E. *et al.* Structural evolution during the reaction of Li with nano-sized rutile type TiO_2 at room temperature. *Electrochem. Commun.* **9,** 337–342 (2007).
42. Hwang, Y.-N., Park, S.-H. & Kim, D. Size-dependent surface phonon mode of CdSe quantum dots. *Phys. Rev. B* **59,** 7285–7288 (1999).
43. Alivisatos, A. P. Semiconductor clusters, nanocrystals and quantum dots. *Science* **271,** 933–937 (1996).
44. Kelly, K. L., Coronado, E., Zhao, L. L. & Schatz, G. C. The optical properties of metal nanoparticles: The influence of size, shape and dielectric environment. *J. Phys. Chem. B* **107,** 668–677 (2003).
45. Pottier, A. S. *et al.* Size tailoring of TiO_2 anatase nanoparticles in aqueous medium and synthesis of nanocomposites. Characterization by Raman spectroscopy. *J. Mater. Chem.* **13,** 877–882 (2003).
46. Chernyshev, A. P. Effect of nanoparticle size on the onset temperature of surface melting. *Mater. Lett.* **63,** 1525–1527 (2009).
47. Zhang, M. *et al.* Size-dependent melting point depression of nanostructures: Nanocalorimetric measurements. *Phys. Rev. B* **62,** 10548–10557 (2000).
48. Sun, J. & Simon, S. L. The melting behavior of aluminium nanoparticles. *Thermochim. Acta* **463,** 32–40 (2007).
49. Dormann, J. L., Fiorani, D. & Tronc, E. Magnetic relaxation in fine-particle systems. *Adv. Chem. Phys.* **98,** 283–494 (1997).
50. Gangopadhyay, S. *et al.* Magnetic properties of ultrafine iron particles. *Phys. Rev. B* **45,** 9778–9787 (1992).
51. Pastor, G. M., Dorantesdavila, J. & Bennemann, K. H. Size and structural dependence of the magnetic properties of small 3d-transition-metal clusters. *Phys. Rev. B* **40,** 7642–7654 (1989).
52. Chen, Q. & Zhang, Z. J. Size-dependent superparamagnetic properties of $MgFe_2O_4$ spinel ferrite nanocrystallites. *Appl. Phys. Lett.* **73,** 3156–3158 (1998).
53. Selbach, S. M., Tybell, T., Einarsrud, M. A. & Grande, T. Size-dependent properties of multiferroic $BiFeO_3$ manoparticles. *Chem. Mater.* **19,** 6478–6484 (2007).
54. Shetty, S., Palkar, V. R. & Pinto, R. Size effect study in magnetoelectric $BiFeO_3$ system. *Pramana* **58,** 1027–1030 (2002).
55. Chattopadhyay, S., Ayyub, P., Palkar, V. R. & Multani, M. Size-induced diffuse phase transition in the nanocrystalline ferroelectric $PbTiO_3$. *Phys. Rev. B* **52,** 13177–13183 (1995).
56. Shih, W. Y., Shih, W.-H. & Aksay, I. A. Size dependence of the ferroelectric transition of small $BaTiO_3$ particles: effect of depolarization. *Phys. Rev. B* **50,** 15575–15585 (1994).
57. Rusanov, A. I. Surface thermodynamics revisited. *Surf. Sci. Rep.* **58,** 111–239 (2005).
58. Borm, P. *et al.* Research strategies for safety evaluation of nanomaterials, Part V: role of dissolution in biological fate and effects of nanoscale particles. *Toxicol. Sci.* **90,** 23–32 (2006).
59. Fan, C., Chen, J., Chen, Y., Ji, J. & Teng, H. H. Relationship between solubility and solubility product: the roles of crystal sizes and crystallographic directions. *Geochim. Cosmochim. Acta* **70,** 3820–3829 (2006).
60. Talapin, D. V., Rogach, A. L., Haase, M. & Weller, H. Evolution of an ensemble of nanoparticles in a colloidal solution: theoretical study. *J. Phys. Chem. B* **105,** 12278–12285 (2001).
61. Rogach, A. L. *et al.* Organization of matter on different size scales: monodisperse nanocrystals and their superstructures. *Adv. Funct. Mater.* **12,** 653–664 (2002).
62. McHale, J. M., Auroux, A., Perrotta, A. J. & Navrotsky, A. Surface energies and thermodynamic phase stability in nanocrystalline aluminas. *Science* **277,** 788–791 (1997).
63. Zhang, H. & Banfield, J. F. Understanding polymorphic phase transformation behavior during growth of nanocrystalline aggregates: insights from TiO_2. *J. Phys. Chem. B* **104,** 3481–3487 (2000).
64. Ranade, M. R. *et al.* Energetics of nanocrystalline TiO_2. *Proc. Natl Acad. Sci. USA* **99,** 6476–6481 (2002).
65. Gratton, S. E. *et al.* The effect of particle design on cellular internalization pathways. *Proc. Natl Acad. Sci. USA* **105,** 11613–11618 (2008).
66. Jiang, W., Kim, B. Y. S., Rutka, J. T. & Chan, W. C. W. Nanoparticle-mediated cellular response is size-dependent. *Nature Nanotech.* **3,** 145–150 (2008).
67. Tao, F. *et al.* Reaction-driven restructuring of Rh–Pd and Pt–Pd core-shell nanoparticles. *Science* **322,** 932–934 (2008).
68. Auffan, M. *et al.* Enhanced adsorption of arsenic onto nano-maghemites: As(III) as a probe of the surface structure and heterogeneity. *Langmuir* **24,** 3215–3222 (2008).
69. Hoyer, P. & Weller, H. Size-dependent redox potentials of quantized zinc oxide measured with an optically transparent thin layer electrode. *Chem. Phys. Lett.* **221,** 379–384 (1994).
70. Yokoyama, A., Komiyama, H., Inoue, H., Masumoto, T. & Kimura, H. M. Hydrogenation of carbon monoxide by amorphous ribbons. *J. Catalys.* **68,** 355–361 (1981).
71. Liu, Y., Choi, H., Dionysiou, D. & Lowry, G. V. Trichloroethene hydrodechlorination in water by highly disordered monometallic nanoiron. *Chem. Mater.* **17,** 5315–5322 (2005).
72. Nurmi, J. T. *et al.* Characterization and properties of metallic iron nanoparticles: spectroscopy, electrochemistry and kinetics. *Environ. Sci. Technol.* **39,** 1221–1230 (2005).
73. Liu, Y., Majetich, S. A., Tilton, R. D., Sholl, D. S. & Lowry, G. V. TCE dechlorination rates, pathways, and efficiency of nanoscale iron particles with different properties. *Environ. Sci. Technol.* **39,** 1338–1345 (2005).
74. Jolivet, J. P. & Barron, A. R. in *Environmental Nanotechnology — Applications and Impacts of Nano-materials* (eds Wiesner, M. R. & Bottero, J. Y.) 29–103 (McGraw Hill, 2007).
75. Banus, E. D., Milt, V. G., Miro, E. E. & Ulla, M. A. Structured catalyst for the catalytic combustion of soot: Co, Ba, K/ZrO_2 supported on Al_2O_3 foam. *Appl. Catalys. A* **362,** 129–138 (2009).
76. Martinez, A., Prieto, G. & Rollan, J. Nanofibrous γ-Al_2O_3 as support for Co-based Fischer-Tropsch catalysts: Pondering the relevance of diffusional and dispersion effects on catalytic performance. *J. Catalys.* **263,** 292–305 (2009).
77. Euzen, P. *et al.* in *Handbook of Porous Materials* (eds Schuth, F., Sing, K. S. W. & Weitkamp, J.) 1591–1677 (Wiley-VCH, 2002).
78. Maira, A. J., Yeung, K. L., Lee, C. Y., Yue, P. L. & Chan, C. K. Size effects in gas-phase photo-oxidation of trichloroethylene using nanometer-sized TiO_2 catalysts. *J. Catalys.* **192,** 185–196 (2000).
79. Wang, C. C., Zhang, Z. & Ying, J. Y. Photocatalytic decomposition of halogenated organics over nanocrystalline titania. *Nanostruct. Mater.* **9,** 583–586 (1997).
80. Almquist, C. B. & Biswas, P. Role of synthesis method and particle size of nanostructured TiO_2 on its photoactivity. *J. Catalys.* **212,** 145–156 (2002).
81. Santra, A. K. & Goodman, D. W. Oxide-supported metal clusters: models for heterogeneous catalysts. *J. Phys. Condens. Matter* **15,** R31–R62 (2003).
82. Daniel, M. C. & Astruc, D. Gold nanoparticles: assembly, supramolecular chemistry, quantum-size-related properties and applications toward biology, catalysis and nanotechnology. *Chem. Rev.* **104,** 293–346 (2004).
83. Haruta, M. Size- and support-dependency in the catalysis of gold. *Catalys. Today* **36,** 153–166 (1997).
84. Sau, T. K., Pal, A. & Pal, T. Size regime dependent catalysis by gold nanoparticles for the reduction of eosin. *J. Phys. Chem. B* **105,** 9266–9272 (2001).
85. Cortie, M. B. & Van der Lingen, E. Catalytic gold nanoparticles. *Mater. Forum* **26,** 1–14 (2002).
86. Turner, M. *et al.* Selective oxidation with dioxygen by gold nanoparticle catalysts derived from 55-atom clusters. *Nature* **454,** 981–983 (2008).
87. Miller, J. T. *et al.* The effect of gold particle size on Au–Au bond length and reactivity toward oxygen in supported catalysts. *J. Catalys.* **240,** 222–234 (2006).
88. Madden, A. S., Hochella, M. F. & Luxton, T. P. Insights for size-dependent reactivity of hematite nanomineral surfaces through Cu^{2+} sorption. *Geochim. Cosmochim. Acta* **70,** 4095–4104 (2006).
89. Villiéras, F. *et al.* Surface heterogeneity of minerals. *C. R. Geosci.* **334,** 597–609 (2002).
90. Yean, S. *et al.* Effect of magnetic particle size on adsorption and desorption of arsenite and arsenate. *J. Mater. Res.* **20,** 3255–3264 (2005).
91. Stumm, W. & Morgan, J. J. *Aquatic Chemistry: An Introduction Emphasizing Chemical Equilibria in Natural Waters* 2nd edn (Wiley-Interscience, 1981).
92. Sigg, L., Behra, P. & Stumm, G. N. *Chimie des Milieux Aquatiques, Chimie des Eaux Naturelles et des Interfaces dans l'Environnement* (Dunod, 2000).
93. Navrotsky, A., Mazeina, L. & Majzlan, J. Size-driven structural and thermodynamic complexity in iron oxides. *Science* **319,** 1635–1638 (2008).
94. Jolivet, J. P. & Tronc, E. Interfacial electron transfer in colloidal spinel iron oxide. Conversion of Fe_3O_4-γ-Fe_2O_3 particles in aqueous medium. *J. Colloid Interface Sci.* **125,** 688–701 (1988).
95. Gurr, J.-R., Wang, A. S. S., Chen, C.-H. & Jan, K.-Y. Ultrafine titanium dioxide particles in the absence of photoactivation can induce oxidative damage to human bronchial epithelial cells. *Toxicology* **213,** 66–73 (2005).

96. Warheit, D. B., Webb, T. R., Sayes, C. M., Colvin, V. L. & Reed, K. L. Pulmonary instillation studies with nanoscale TiO2 rods and dots in rats: Toxicity is not dependent upon particle size and surface area. *Toxicol. Sci.* **91,** 227–236 (2006).
97. Hirakawa, K., Mori, M., Yoshida, M., Oikawa, S. & Kawanishi, S. Photo-irradiated titanium dioxide catalyzes site specific DNA damage via generation of hydrogen peroxide. *Free Radic. Res.* **38,** 439–447 (2004).
98. Sato, T. & Taya, M. Enhancement of phage inactivation using photocatalytic titanium dioxide particles with different crystalline structures. *Biochem. Eng. J.* **28,** 303–308 (2006).
99. Jang, H. D., Kim, S.-K. & Kim, S.-J. Effect of particle size and phase composition of titanium dioxide nanoparticles on the photocatalytic properties. *J. Nanopart. Res.* **3,** 141–147 (2001).
100. Braydich-Stolle, L. *et al.* Crystal structure mediates mode of cell death in TiO_2 nanotoxicity. *J. Nanopart. Res.* **11,** 1361–1374 (2009).
101. Auffan, M., Rose, J., Wiesner, M. R. & Bottero, J. Y. Chemical stability of metallic nanoparticles: a parameter controlling their potential toxicity *in vitro*. *Environ. Pollut.* **157,** 1127–1133 (2009).
102. Brunner, T. J. *et al. In vitro* cytotoxicity of oxide nanoparticles: comparison to asbestos, silica, and the effect of particle solubility. *Environ. Sci. Technol.* **40,** 4374–4381 (2006).
103. Pourbaix, M. *Atlas of Electrochemical Equilibria in Aqueous Solutions* (US National Association of Corrosion Engineers, 1974).
104. Franklin, N. M. *et al.* Comparative toxicity of nanoparticulate ZnO, bulk ZnO, and $ZnCl_2$ to a freshwater microalga (*Pseudokirchneriella subcapitata*): the importance of particle solubility. *Environ. Sci. Technol.* **41,** 8484–8490 (2007).
105. Derfus, A. M., Chan, W. C. W. & Bhatia, S. N. Probing the cytotoxicity of semiconductor quantum dots. *Nano Lett.* **4,** 11–18 (2004).
106. Morones, J. R. *et al.* The bactericidal effect of silver nanoparticles. *Nanotechnology* **16,** 2346–2353 (2005).
107. Wang, S. *et al.* Challenge in understanding size and shape dependent toxicity of gold nanomaterials in human skin keratinocytes. *Chem. Phys. Lett.* **463,** 145–149 (2008).
108. Park, E. J., Choi, J., Park, Y. K. & Park, K. Oxidative stress induced by cerium oxide nanoparticles in cultured BEAS-2B cells. *Toxicology* **245,** 90–100 (2008).

Acknowledgements

This material is based on work supported by the US National Science Foundation (NSF) and Environmental Protection Agency (EPA) under an NSF Cooperative Agreement (EF-0830093, Center for Environmental Implications of NanoTechnology). The French Atomic Energy Commission (CEA) and National Center for Scientific Research (CNRS) are acknowledged for their support and funding of the international Consortium for the Environmental Implications of Nanotechnology. This work has also been funded by the French National Program ANR and ACI-FNS ECCO supported by the French National Institute for Earth Sciences and Astronomy.